Density-functional theory for the structures and thermodynamic properties of highly asymmetric electrolyte and neutral component mixtures

Zhidong Li and Jianzhong Wu*
Department of Chemical and Environmental Engineering, University of California, Riverside, California 92521-0425, USA
(Received 26 January 2004; revised manuscript received 7 May 2004; published 24 September 2004)

Density-functional theory (DFT) is applied to investigate the structural and thermodynamic properties of concentrated electrolyte and neutral component mixtures that are highly asymmetric in terms of both size and charge mimicking a crowded cellular environment. The excess Helmholtz energy functional is derived from a modified fundamental measure theory for the hard-sphere repulsion and a quadratic functional Taylor expansion for the electrostatic interactions. The direct correlation functions are obtained from the analytical solutions of the mean-spherical approximation. In the context of a primitive model where biomacromolecules are represented by neutral or charged hard spheres and the solvent is represented by a continuous dielectric medium, this DFT is able to take into account both the excluded-volume effects and the long-ranged electrostatic interactions quantitatively. The performance of the theoretical method has been tested with Monte Carlo simulation results from this work and from the literature for the pair correlation functions, excess internal energies, and osmotic coefficients for a wide variety of aqueous dispersions of charged and neutral particles.

DOI: 10.1103/PhysRevE.70.031109 PACS number(s): 82.60.−s, 05.70.−a

I. INTRODUCTION

There has been growing interest in recent years to study the structural and thermodynamic properties of macroion dispersions in the presence of neutral species. Such systems provide a primitive model for a crowded cellular environment that contains numerous biomacromolecules and cellular polymers [1,2]. The so-called "macromolecular crowding" affects many aspects of cellular functions and biomacromolecular properties including protein stability, association, enzymatic activity, and diffusion. For instance, biomacromolecules at a high concentration play an important role in many diseases, including cataract in eye lens, sickle cell anemia, and so forth that are caused by the condensation of proteins [3]. Dispersions of macroions and neutral species are also relevant to traditional applications such as in the selective precipitation or purification of proteins by addition of neutral polymers [4].

In a primitive model where biomacromolecules are represented by charged and neutral species, the properties of macromolecular crowding are primarily determined by the excluded-volume effects and the long-ranged Coulomb interactions. A wide variety of theoretical and simulation techniques, including the symmetric Poisson-Boltzmann (SPB) equation, modified Poisson-Boltzmann (MPB) equation, and the hypernetted chain (HNC) approximation, have been used to investigate the structural and thermodynamic properties of macromolecular crowding systems within the primitive model [5–9]. Among these theories, HNC performs better than Poisson-Boltzmann (PB) type approaches but it has convergence problems for strongly asymmetric systems [6].

Density-functional theory (DFT) represents a powerful alternative to the Poisson-Boltzmann equation and integral-equation theories with even higher accuracy, more convenience for calculations and broader applications. A comprehensive comparison of DFT with various conventional theories for describing the structures and thermodynamics of electric double layers has been published earlier [10]. Very recently, Kinjo and Takad used DFT to study the effect of macromolecular crowding on the static and dynamic properties of protein folding and aggregation in a neutral solution environment [11,12]. They concluded that the addition of a crowding agent will stabilize native proteins and enhance the aggregation of denatured proteins, in good agreement with experiments qualitatively. As in many other previous investigations on macromolecular crowding, this work is primarily concerned with the excluded-volume effects; all other intermolecular interactions are neglected. In the present work, we propose a quantitative density-functional theory that accounts for both excluded volume and electrostatic interactions. This theory is expected to be more useful than the hard-sphere model for predicting the structural and thermodynamic properties of macromolecular crowding. The excess free-energy functional due to the short-ranged repulsion is evaluated through a modified fundamental measure theory (MFMT) that has been proved to be very accurate for hard-sphere fluids [13–15]. The electrical contribution is calculated using a quadratic functional Taylor expansion of the Helmholtz energy functional [10]. The theoretical predictions are tested with extensive computer simulation data for the corresponding model systems.

The present density-functional theory has a number of advantages in comparison with the conventional approaches. First, it utilizes an accurate free-energy functional for hard spheres, which is important for macromolecular crowding where the excluded volume effects are significant. Although the quadratic density-functional expansion is essentially equivalent to HNC, such expansion applies only to the electrostatic part in the present version of density-functional theory, but to both hard-sphere and electrostatic interactions

*Author to whom correspondence should be addressed. Email address: jwu@engr.ucr.edu

in HNC. In addition, the extension of the DFT approach to include other forms of intermolecular potentials such as dispersion, association, and polymeric molecules is relatively straightforward. Such extension is less obvious in more traditional theories. However, inclusions of nonprimitive interactions are expected to be important for a refined theory of macromolecular crowding. Although DFT has its own limitations at low electrolyte concentrations (inherited from the direct correlation function) and for systems with strong electrostatic interactions, it provides accurate thermodynamic properties at least as good as HNC and much better than SPB and MPB. From a methodological point of view, this work represents the first application of the residual direct correlation function (DCF) from the mean-spherical approximation (MSA) to highly asymmetric electrolyte solutions.

The remainder of this paper is organized as follows. We first introduce the basic formulism of the DFT for asymmetric electrolytes. Then it follows the application of DFT to dispersions of neutral species and macroions in electrolyte solutions. Specifically, we consider systems with the size ratio of macroions, counterions and neutral particles equal to 10:1:4 (4 nm/0.4 nm/1.6 nm), and the valence ratio between macroions and counterions ranging from 6:1 to 15:3. Apart from the structural properties as represented by the pair correlation functions, we have also investigated the performance of the DFT in comparison with that of HNC, SPB, and MPB for predicting the excess internal energies and osmotic coefficients of dispersions with different concentrations of neutral species and electrolytes as well as at different valences of macroions and counterions.

II. DENSITY-FUNCTIONAL THEORY

We consider model macromolecular crowding systems consisting of spherical macroions and neutral particles dispersed in an electrolyte solution. The macroions and neutral species provide a coarse-grained representation of biomacromolecules in a cellular environment. As in the primitive model of electrolyte solutions, the macroions and small ions are represented by charged hard spheres and the solvent is modeled as a continuous dielectric medium. The pair potential $u_{ij}(r)$ between two species i and j is given by

$$u_{ij}(r) = \begin{cases} \infty, & r < \sigma_{ij} \\ \dfrac{Z_i Z_j e^2}{\varepsilon r}, & r \geqslant \sigma_{ij} \end{cases}, \tag{1}$$

where e is the electron charge, Z_i and σ_i are the valence and diameter of particle i, respectively, $\sigma_{ij}=(\sigma_i+\sigma_j)/2$, and r is the center-to-center distance between the particles. For a neutral particle, the valence is zero and the pair potential is reduced to that for two hard spheres. In Eq. (1), $\varepsilon=4\pi\varepsilon_0\varepsilon_r$ stands for the dielectric constant of the solvent with ε_0 being the vacuum permittivity and ε_r being the solvent relative permittivity. We use $\varepsilon_r=78.4$ in all our calculations, corresponding to that for pure water at 298.15 K. As in most previous investigations of macroion systems, we neglect the dielectric discontinuity at the macroion surface. Recently, the effect of image charges for spherical colloids has been thoroughly discussed by Messina [16].

The central task of a density-functional theory is to derive an analytical expression for the grand potential of an open system as a functional of the density profiles. In general, the grand potential is related to the intrinsic Helmholtz energy functional $F[\{\rho_i(\mathbf{r})\}]$ via the Legendre transformation

$$\Omega[\{\rho_i(\mathbf{r})\}] = F[\{\rho_i(\mathbf{r})\}] + \sum_{i=1}^{N} \int d\mathbf{r}\rho_i(\mathbf{r})[V_i(\mathbf{r}) - \mu_i], \tag{2}$$

where $\{\rho_i(\mathbf{r})\}$ is a set of density profiles for all species, N is the number of components, μ_i is the chemical potential, and $V_i(\mathbf{r})$ is the external potential. For a uniform system as considered in this work, the external potential $V_i(\mathbf{r})$ can be introduced by fixing a particle in the origin. In that case, the density profiles divided by the average densities correspond to the pair distribution functions around the fixed particle.

For a mixture of charged and neutral particles, the intrinsic Helmholtz energy functional F can be decomposed into four parts, i.e., [17–20],

$$F[\{\rho_i(\mathbf{r})\}] = F^{id}[\{\rho_i(\mathbf{r})\}] + F_{hs}^{ex}[\{\rho_i(\mathbf{r})\}] + F_C^{ex}[\{\rho_i(\mathbf{r})\}] + F_{el}^{ex}[\{\rho_i(\mathbf{r})\}], \tag{3}$$

where $F^{id}[\{\rho_i(\mathbf{r})\}]$ is the corresponding intrinsic Helmholtz energy for an ideal gas, $F_{hs}^{ex}[\{\rho_i(\mathbf{r})\}]$ represents the contribution due to the hard-sphere repulsions, $F_C^{ex}[\{\rho_i(\mathbf{r})\}]$ is the direct Coulomb energy, and $F_{el}^{ex}[\{\rho_i(\mathbf{r})\}]$ represents correlations due to Coulomb and hard-sphere interactions. The ideal-gas term $F^{id}[\{\rho_i(\mathbf{r})\}]$ is known exactly,

$$\beta F^{id}[\{\rho_i(\mathbf{r})\}] = \sum_{i=1}^{N} \int d\mathbf{r}\rho_i(\mathbf{r})\{\ln(\rho_i(\mathbf{r})\lambda_i^3) - 1\}, \tag{4}$$

where λ denotes the thermal wavelength and $\beta=1/k_BT$, with k_B being the Boltzmann constant and T being the absolute temperature. The direct Coulomb term $F_C^{ex}[\{\rho_i(\mathbf{r})\}]$ is given by

$$\beta F_C^{ex}[\{\rho_i(\mathbf{r})\}] = \frac{1}{2}\int\int d\mathbf{r}\, d\mathbf{r}' \sum_{i,j} \frac{Z_i Z_j e^2 \rho_i(\mathbf{r})\rho_j(\mathbf{r}')}{\varepsilon k_B T|\mathbf{r}-\mathbf{r}'|}. \tag{5}$$

The intrinsic Helmholtz energy functional due to the hard-sphere repulsions $F_{hs}^{ex}[\{\rho_i(\mathbf{r})\}]$ is represented by a modification of Rosenfeld's fundamental measure theory [21,22],

$$\beta F_{hs}^{ex} = \int \Phi^{hs}[n_\alpha(\mathbf{r})]d\mathbf{r}, \tag{6}$$

where the reduced excess Helmholtz energy density Φ^{hs} is given by

$$\Phi^{hs} = -n_0\ln(1-n_3) + \frac{n_1 n_2 - \mathbf{n}_{V1}\cdot\mathbf{n}_{V2}}{1-n_3} + \frac{1}{36\pi}\left[n_3\ln(1-n_3) + \frac{n_3^2}{(1-n_3)^2}\right]\left(\frac{n_2}{n_3}\right)^3\left(1-\frac{\mathbf{n}_{v2}^2}{n_2^2}\right)^3. \tag{7}$$

The detailed expressions for the weighted densities, $n_\alpha(\mathbf{r})$, $\alpha=0,1,2,3,V1,V2$, can be found in our previous publications or in Rosenfeld's original work [14,15,23]. In the bulk limit, the two vector weighted densities $\mathbf{n}_{V1}$ and $\mathbf{n}_{V2}$ vanish

and the Helmholtz free-energy density $\mathbf{\Phi}^{hs}$ becomes identical to that from the Boublik-Mansoori-Carnahan-Starling-Leland (BMCSL) equation of state [24,25].

To obtain an expression for the residual Helmholtz free-energy functional $F_{el}^{ex}[\{\rho_i(\mathbf{r})\}]$ due to the electrostatic interactions and intermolecular correlations, we make a quadratic functional Taylor expansion around the bulk densities $\{\rho_i^b\}$ by neglecting all higher-order terms

$$\beta F_{el}^{ex}[\{\rho_i(\mathbf{r})\}] = \beta F_{el}^{ex}[\{\rho_i^b\}] - \int d\mathbf{r} \sum_{i=1}^{N} \Delta C_i^{(1)el}[\rho_i(\mathbf{r}) - \rho_i^b] - \frac{1}{2}\int\int d\mathbf{r}\, d\mathbf{r}' \sum_{j=1}^{N}\sum_{i=1}^{N} \Delta C_{ij}^{(2)el}(|\mathbf{r}-\mathbf{r}'|) \times [\rho_i(\mathbf{r}) - \rho_i^b][\rho_j(\mathbf{r}') - \rho_j^b], \quad (8)$$

where the DCFs are defined as

$$\Delta C_1^{(1)el} = -\ \delta\beta F_{el}^{ex}/\delta\rho_i(\mathbf{r})|_b, \quad (9)$$

$$\Delta C_{ij}^{(2)el}(|\mathbf{r}-\mathbf{r}'|) = -\ \delta^2\beta F_{el}^{ex}/\delta\rho_i(\mathbf{r})\,\delta\rho_j(\mathbf{r}')|_b. \quad (10)$$

The first term on the left-hand side of Eq. (8) corresponds to the electrostatic part of the excess Helmholtz energy for a uniform fluid and the third term takes into account correlations among ion distributions. Because the direct Coulomb term is explicitly taken into account in Eq. (5), the two-body excess direct correlation function is given by

$$\Delta C_{ij}^{(2)el}(r) = C_{ij}(\mathbf{r}) + \frac{\beta Z_i Z_j e^2}{\varepsilon r} - C_{ij}^{hs}(\mathbf{r}). \quad (11)$$

In this work, $\Delta C_{ij}^{(2)el}(r)$ is calculated from the analytical expressions derived from the MSA[26]. The expressions for the two-body direction correlation functions of electrolyte solutions from MSA are reproduced in the appendix.

The pair correlation functions (PCF) in a uniform highly asymmetric mixture can be calculated using the Percus' test-particle method. The idea is that the system is invariant when a particle is fixed at the origin; the pair correlation functions are equivalent to the reduced density profiles of other species around the fixed particle. As the grand potential $\Omega[\{\rho_i(\mathbf{r})\}]$ reaches a minimum at equilibrium, the pair correlation function $g_{ij}(r)$ satisfies the Euler-Lagrange equation

$$-k_BT\ln[g_{ij}(\mathbf{r})] = -k_BT\ln\left[\frac{\rho_j(\mathbf{r})}{\rho_j^b}\right] = \left[\frac{\delta F_{hs}^{ex}}{\delta\rho_j(\mathbf{r})} - \mu_{j,hs}^{ex}\right] + Z_j e[\psi_i(\mathbf{r}) - \psi_i^b] - k_BT\sum_{k=1}^{N}\int [\rho_k(\mathbf{r}') - \rho_k^b]\Delta C_{jk}^{(2)el} \times (|\mathbf{r}-\mathbf{r}'|)d\mathbf{r}', \quad (12)$$

where $\psi_i(\mathbf{r})$ stands for the mean-electrostatic potential. In the spherical coordinates, the mean-electrostatic potential can be expressed as

$$\psi_i(r) = \frac{4\pi e}{\varepsilon}\int_r^\infty \sum_{k=1}^{N} \rho_k(r')Z_k\left[r' - \frac{r'^2}{r}\right]dr', \quad (13)$$

where r is the distance to the center of the fixed particle. From the condition of electrostatic neutrality, we have

$$Z_i = -4\pi\sum_{k=1}^{N}\int_{\sigma_{ik}}^{\infty} \rho_k(r)Z_k r^2 dr, \quad (14)$$

where Z_j and σ_i are the valence and diameter of the fixed particle, respectively. Equation (12) can be solved self-consistently using the Picard iteration. Once we have the pair correlation functions, all thermodynamic properties of the system can be calculated following the standard statistical-mechanical equations.

III. MONTE CARLO SIMULATIONS

Besides the simulation data from the literature [6], *NVT*-ensemble Monte Carlo simulations are also carried out in this work to test the performance of the DFT for systems containing 15:*n* ($n=1/2/3$) electrolyte-neutral component mixtures and 6:1 pure electrolyte. For 15:*n* systems, the cubic simulation box contains 20 macroions, 300/150/100 neutralizing counterions depending on the valence, and 3000 neutral particles. The corresponding concentrations of electrolyte and neutral component are $C_e=0.002M$ and $C_0=0.3M$, respectively. The periodical boundary conditions are applied to each dimension of the simulation box and the Ewald sum method is used to account for the long-ranged Coulomb interactions [27]. The system is claimed at equilibrium after 10^5 Monte Carlo steps per particle and another 2×10^5 configurations are used to calculate the ensemble averages.

IV. RESULTS AND DISCUSSION

A. Microscopic structure

The systems considered in this work consist of an electrolyte and a neutral species that are highly asymmetric in both size and valence. The diameters of cations, anions, and neutral particles are 4, 0.4, and 1.6 nm, respectively. These systems provide a primitive model for the so-called "macromolecular crowding" environment. We first test the performance of DFT for predicting the microscopic structures of such mixtures. The subscripts "++," "−−," "+−," "0+," "0−" and "00" designate macroion-macroion, counterion-counterion, macroion-counterion, neutral-macroion, neutral-counterion, and neutral-neutral pair correlation functions, respectively. The Monte Carlo simulation data are from either Ref. [6] or this work.

Figure 1 shows the DFT predictions for solutions of 6:1 electrolyte without or with a neutral component. Here the molar concentration of the electrolyte is $C_e=0.002M$ and that for the neutral species is $C_0=0.1M$, corresponding to a packing (volume) fraction of $\eta_0=0.129$. In general, the theoretical predictions are in very good agreement with simulation results. The correlations between like- or unlike-charged ions are similar to those in a simple electrolyte solution. In accor-

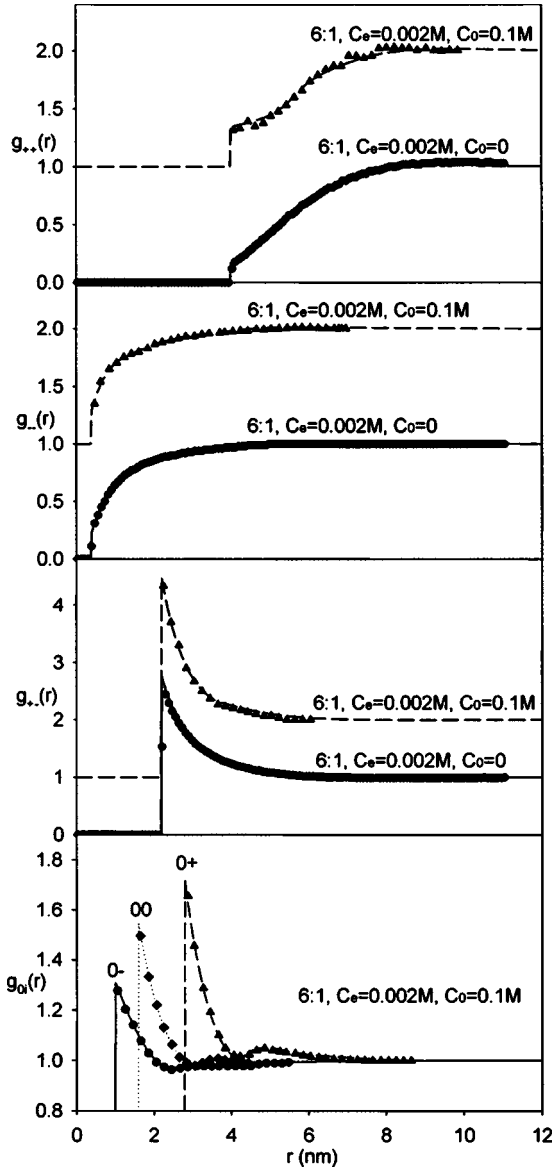

FIG. 1. Structures of 6:1 electrolyte ($C_e=0.002M$) without or with neutral species ($C_0=0.1M$). Symbols represent MC results from this work and from Ref. [6]. For clarity, the macroion-macroion, counterion-counterion, and macroion-counterion pair correlation functions with neutral component have been shifted upward by one unit.

dance with the prediction of the Poisson-Boltzmann equations, the density profiles of macroions and microions around a fixed ion are monotonic, with a significant accumulation of counterions accompanied by a depletion of coions. The presence of the neutral component attenuates the correlations between like-charged ions but strengthens those between unlike-charged ions. Because of the excluded-volume effects, macroions, counterions, and neutral particles all accumulate to the neutral particle surface and the degree of accumulation is directly related to the particle size.

Figure 2 presents the effects of counterion valence on the pair correlation functions at a fixed macroion charge (+6). Here the concentrations of electrolyte and neutral component remain at $C_e=0.002M$ and $C_0=0.1M$ and the counterion valence can be monovalent, divalent, and trivalent. As the counterion valence increases, the accumulation of counterions near the macroion surface becomes more evident, accompanied by a stronger repulsion between counterions. However, the long-range correlation between macroions diminishes with the increase in the counterion valence, indicating a stronger screening of the macroions by counterions. The DFT faithfully reproduces the MC results when the system contains monovalent counterions. For systems containing multivalent counterions (6:2 and 6:3), however, the accuracy of DFT deteriorates. In particular, it underestimates the contact values of the macroion-macroion pair distribution functions. At the small separation of macroions, the correlation is probably also sensitive to the macroion-counterion-macroion three-body interaction that is ignored in the quadratic expansion.

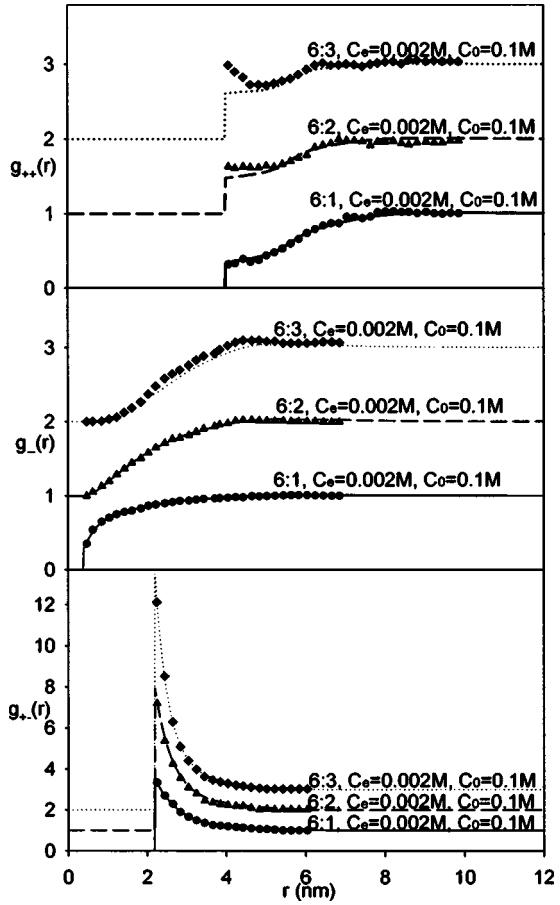

FIG. 2. Macroion-macroion, counterion-counterion, and macroion-counterion pair correlation functions for 6:n ($n=1,2,3$) electrolyte ($C_e=0.002M$) and neutral component ($C_0=0.1M$) mixtures. Symbols represent MC results from Ref. [6]. As in Fig. 1, the curves for 6:2 and 6:3 have been consecutively shifted upward by one unit.

Next, we consider a more complicated situation that involves macroions of higher valence (+15). The counterion valence is also changed from monovalent to trivalent. The concentrations of electrolyte and neutral component are at $C_e=0.002M$ and $C_0=0.3M$ respectively. Under these concentrations, the total packing fraction reaches 0.43, very close to

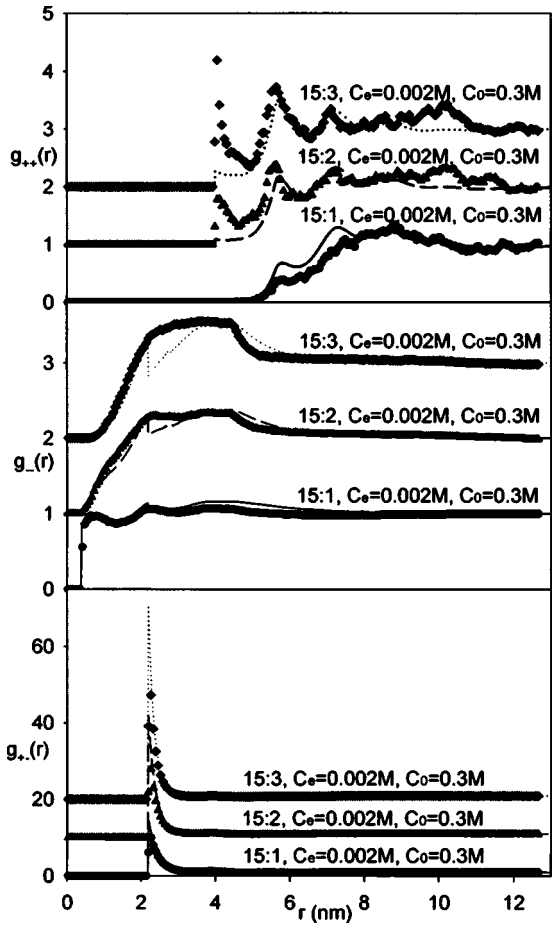

FIG. 3. Same as Figure 2 but for 15:n ($n=1,2,3$) electrolyte ($C_e=0.002M$) and neutral component ($C_0=0.3M$) mixtures. Symbols represent MC results also from this work. The macroion-counterion pair correlation functions for 15:2 and 15:3 have been shifted upward by 10 and 20, respectively.

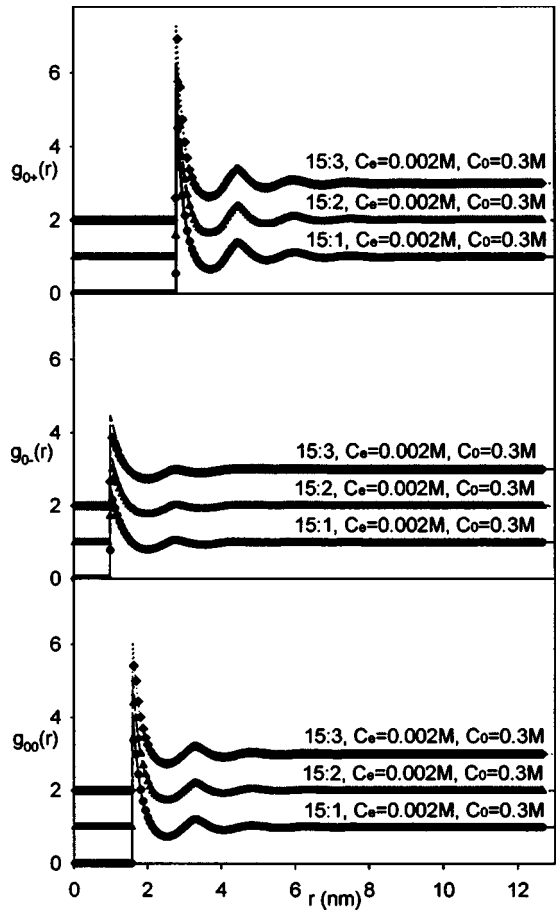

FIG. 4. Macroion-neutral, counterion-neutral, and neutral-neutral pair correlation functions for 15:n ($n=1,2,3$) electrolyte ($C_e=0.002M$) and neutral component ($C_0=0.3M$) mixtures. Symbols represent MC results also from this work. For clarity, the curves for 15:2 and 15:3 have been shifted upward by 1 and 2, respectively.

the solidification of the mixture. Figures 3 and 4 show all the pair correlation functions at different valences of counterions. In Fig. 3, we observed that, as in Fig. 2, the depletion between counterions and the accumulation between unlike-charged ions become stronger, but the correlation between macroions is weakened with the increase of the counterion valence. Figure 4 indicates that the change of counterion valence has only minor influence on the distributions of macroions, counterions, and neutral particles near the surface of a fixed neutral particle. The DFT agrees with MC fairly well for predicting the macroion-counterion, macroion-neutral, counterion-neutral, and neutral-neutral distributions under all the three conditions. But for stronger electrostatic interactions, i.e., in 15:2 and 15:3 solutions, the DFT fails for the macroion-macroion and counterion-counterion correlation functions. In addition to a significant underestimation of the contact values of the macroion-macroion distributions as shown in Fig. 2, the DFT erroneously predicts a discontinuity of the counterion-counterion distributions. This discontinuity is probably related to the inaccuracy of the DCFs from MSA, in particular, at low concentrations of electrolytes.

B. Thermodynamic properties

With the pair correlation functions presented above, it is relatively straightforward to calculate the thermodynamic properties of highly asymmetric electrolyte-neutral species mixtures. The reduced excess internal energy per particle is given by [28]

$$\frac{\beta E^{ex}}{N_t} = \frac{1}{2}\rho_t \sum_{i=1}^{N}\sum_{j=1}^{N} x_i x_j \int 4\pi r^2 g_{ij}(r)\beta u_{ij}(r)dr, \qquad (15)$$

where N_t is the total number of all particles, ρ_t is the total number density in the bulk, and x_i represents the molar faction of particle i. The osmotic coefficient can be obtained via the virial pressure equation [29]

$$\phi = 1 + \frac{\beta E^{ex}}{3N_t} + \frac{2\pi\rho_t}{3}\sum_{i=1}^{N}\sum_{j=1}^{N} x_i x_j \sigma_{ij}^3 g_{ij}(\sigma_{ij}). \qquad (16)$$

Tables I and II present the excess internal energies and osmotic coefficients of a variety of electrolyte mixtures from

TABLE I. Reduced excess internal energy and osmotic coefficient calculated from MC, DFT, HNC, SPB, and MPB at a variety of solution conditions. MC, HNC, SPB, and MPB results are from Ref. [6].

				Excess internal energy					Osmotic coefficient				
Z_+	$C_0(M)$	Z_-	$C_e(M)$	MC	DFT	HNC	SPB	MPB	MC	DFT	HNC	SPB	MPB
+6	0	−1	0.002	0.552	0.558	0.550	0.491	0.513	0.941	0.944	0.943	0.970	0.954
			0.005	0.682	0.697	0.683	0.600	0.633	1.06	1.07	1.06	1.17	1.09
		−2	0.002	1.28	1.30	1.27	1.12	1.19	0.802	0.802	0.806	0.839	0.819
			0.005	1.55	1.58	1.55	1.33	1.42	0.920	0.930	0.925	1.06	0.967
		−3	0.002	2.13	2.13	2.12	1.84	1.99	0.670	0.650	0.666	0.699	0.678
			0.005	2.52	2.51	2.52	2.11	2.29	0.771	0.777	0.783	0.929	0.839
	0.1	−1	0.002	0.0683	0.0703	0.0688	0.0613	0.0644	1.90	1.90	1.94	1.93	1.92
			0.005	0.182	0.186	0.180	0.158	0.168	2.22	2.22	2.31	2.37	2.28
		−2	0.002	0.0954	0.0992	0.0962	0.0847	0.0907	1.92	1.92	1.97	1.95	1.94
			0.005	0.266	0.271	0.264	0.225	0.244	2.28	2.28	2.39	2.42	2.35
		−3	0.002	0.121	0.123	0.122	0.106	0.116	1.93	1.93	1.97	1.96	1.94
			0.005	0.334	0.337	0.335	0.280	0.307	2.30	2.30	2.41	2.42	2.37
+8	0	−1	0.002	0.792	0.807	0.776	0.687	0.726	0.890	0.897	0.899	0.930	0.907
			0.005	0.960	0.982	0.961	0.828	0.883	1.00	1.01	1.01	1.15	1.04
		−2	0.002	1.86	1.91	1.85	1.57	1.70	0.709	0.703	0.711	0.747	0.725
			0.005	2.19	2.23	2.19	1.83	1.99	0.807	0.825	0.818	0.972	0.866
	0.1	−1	0.002	0.122	0.126	0.123	0.106	0.113	1.87	1.87	1.91	1.93	1.90
			0.005	0.302	0.314	0.304	0.260	0.280	2.16	2.15	2.24	2.37	2.24
		−2	0.002	0.172	0.179	0.171	0.145	0.158	1.90	1.90	1.94	1.95	1.92
			0.005	0.447	0.461	0.447	0.370	0.408	2.22	2.22	2.32	2.42	2.32
+10	0	−1	0.002	1.05	1.07	1.04	0.883	0.940	0.839	0.852	0.849	0.893	0.862
			0.005	1.25	1.28	1.25	1.05	1.14	0.953	0.970	0.958	1.14	0.993
		−2	0.002	2.47	2.56	2.46	2.01	2.21	0.620	0.613	0.628	0.659	0.636
			0.005	2.84	2.91	2.85	2.32	2.56	0.713	0.735	0.726	0.897	0.778
	0.1	−1	0.002	0.194	0.199	0.186	0.161	0.173	1.84	1.84	1.88	1.92	1.88
			0.005	0.451	0.467	0.451	0.378	0.412	2.08	2.09	2.17	2.38	2.20
		−2	0.002	0.270	0.282	0.267	0.218	0.243	1.87	1.87	1.92	1.94	1.91
			0.005	0.669	0.693	0.670	0.541	0.605	2.16	2.16	2.25	2.42	2.28
	$F_{\mathrm{div}}(\%)$			...	2.44	0.65	14.92	8.16	...	0.70	2.07	8.70	3.34

MC simulation, DFT, HNC, SPB, and MPB. Here the MC, HNC, MPB, and SPB results are from Ref. [6]. To evaluate the overall performance of various theories, we calculate the average deviation for all systems shown in Tables I and II

$$F_{div}(\%) = \frac{1}{N}\sum_{i=1}^{N}\left|\frac{\theta^{TH}-\theta^{MC}}{\theta^{MC}}\right| \times 100\%, \qquad (17)$$

where θ^{TH} and θ^{MC} are the values predicted by the theory and MC simulation, respectively, and N is the total number of systems investigated. The average deviation for the excess internal energies predicted by DFT is slightly higher than those from HNC but much lower than those from PB equations. For osmotic coefficients, the DFT is the best among the four theories and the predicted results agree very well with simulations. When the electrolyte concentration reaches 0.01 M, the performances of HNC, SPB, and MPB significantly deteriorate but the DFT remains highly accurate.

From these two tables, we may make the following conclusions. First, the addition of neutral species increases both the excess internal energy and the osmotic coefficient. Second, an increase in the electrolyte concentration will reduce the excess internal energy but raise the osmotic coefficient. Third, both the excess internal energy and osmotic coefficient decline with the increase of the macroion valence. Finally, for pure electrolytes the osmotic coefficient falls as the counterion valence increases, but the opposite is true for electrolyte-neutral component mixtures, and the excess internal energy always falls with increasing counterion valence.

In Table III, we compare the excess internal energies and osmotic coefficients from Monte Carlo simulations and from DFT for 15:n (n=1,2,3) electrolyte and neutral component mixtures corresponding to those shown in Figs. 3 and 4. Although the DFT has some limitations in predicting the microscopic structures, it provides accurate thermodynamic properties because at low concentration of the electrolyte, the

TABLE II. Reduced excess internal energy and osmotic coefficient calculated from MC, DFT, HNC, SPB, and MPB for 6:*n* ($n=1,2,3$) electrolyte ($C_e=0.01M$) under different concentration of neutral component ($C_0=0, 0.05M, 0.1M, 0.15M$). MC, HNC, SPB, and MPB results are from Ref. [6].

		Excess internal energy					Osmotic coefficient				
Z_-	$C_0(M)$	MC	DFT	HNC	SPB	MPB	MC	DFT	HNC	SPB	MPB
−1	0	0.803	0.815	0.784	0.700	0.729	1.35	1.37	1.38	1.72	1.42
	0.05	0.470	0.484	0.464	0.411	0.430	2.05	2.06	2.15	2.45	2.17
	0.1	0.335	0.325	0.330	0.292	0.307	3.03	3.05	3.32	3.43	3.20
	0.15	0.263	0.277	0.257	0.228	0.240	4.53	4.53	5.23	4.88	4.75
−2	0	1.80	1.82	1.79	1.50	1.60	1.24	1.29	1.29	1.67	1.36
	0.05	0.811	0.825	0.803	0.674	0.721	2.14	2.16	2.27	2.52	2.29
	0.1	0.527	0.542	0.521	0.437	0.470	3.22	3.23	3.55	3.55	3.41
	0.15	0.393	0.411	0.388	0.324	0.351	4.81	4.82	5.59	5.08	5.06
−3	0	2.88	2.86	2.88	2.33	2.52	1.14	1.16	1.16	1.58	1.30
	0.05	1.09	1.09	1.09	0.881	0.958	2.17	2.19	2.30	2.52	2.35
	0.1	0.679	0.687	0.676	0.546	0.598	3.28	3.30	3.64	3.57	3.49
	0.15	0.496	0.509	0.493	0.398	0.438	4.92	4.93	5.72	5.12	5.17
$F_{\text{div}}(\%)$		...	2.29	1.03	16.44	10.56	...	0.97	8.64	16.98	6.93

thermodynamic properties become insensitive to the microscopic structures.

V. CONCLUSIONS

We have tested the performance of DFT for predicting the pair correlation functions, excess internal energies, and osmotic coefficients of macroion-neutral particle dispersions by extensive comparison with the Monte Carlo simulation results. Due to the limitation of MSA at very low electrolyte concentration and quadratic expansion, the DFT is unable to reproduce the macroion-macroion and counterion-counterion pair correlation functions faithfully for systems with strong electrostatic interactions. However, even under these circumstances, the DFT still captures all the other pair correlation functions and the thermodynamic properties successfully. The limitation of the DFT at low electrolyte concentration may be eliminated by using a more accurate direct correlation functions.

A theoretical investigation of the so-called "macromolecular crowding" requires many drastic approximations regarding both biomacromolecules and the solution conditions as encountered in a typical cellular environment. Although the primitive model discussed in this work may not completely reflect many aspects of real systems, it represents at least a significant step forward toward understanding macromolecular crowding beyond merely the excluded-volume considerations. In our previous works, we have demonstrated that, in principle, the DFT can be directly extended to include, chain connectivity [30–32], intermolecular associations [33], and van der Waals attractions quantatively [32,34]. Because of its versatility to account for various intermolecular forces, the DFT approach appears promising for further theoretical study of macromolecular crowding under more realistic situations.

TABLE III. Reduced excess internal energy and osmotic coefficient calculated from MC and DFT for 15:*n* ($n=1,2,3$) electrolyte ($C_e=0.002M$) and neutral component ($C_0=0.3M$) mixtures.

	Excess internal energy		Osmotic coefficient	
Z_-	MC	DFT	MC	DFT
−1	0.178	0.189	7.42	7.42
−2	0.286	0.252	7.59	7.60
−3	0.328	0.293	7.64	7.66

ACKNOWLEDGMENTS

We thank Professor Yang-xin Yu at Tsinghua University for technical assistance. This work was supported by the National Science Foundation (CTS-0340948 and CTS 0406100).

APPENDIX: DIRECT CORRELATION FUNCTIONS FROM THE MSA

According to the MSA, the two-body direct correlation functions are

$$C_{ij}(r) = C_{ij}^{hs}(r) - \frac{2\beta e^2}{\varepsilon}[-Z_iN_j + X_i(N_i + \Gamma X_i) - (\sigma_i/3)(N_i + \Gamma X_i)^2], \quad \text{(A1)}$$

when $\sigma_i < \sigma_j$ and $0 \leqslant r \leqslant (\sigma_j - \sigma_i)/2$ or

$$rC_{ij}(r) - rC_{ij}^{hs}(r) = \frac{\beta e^2}{\varepsilon}\left\{\begin{array}{l}(\sigma_i-\sigma_j)\left\{\begin{array}{c}\dfrac{(X_i+X_j)}{4}[(N_i+\Gamma X_i)-(N_j+\Gamma X_j)]\\ -\dfrac{(\sigma_i-\sigma_j)}{16}[(N_i+\Gamma X_i+N_j+\Gamma X_j)^2-4N_iN_j]\end{array}\right\}\\ -r\left\{\begin{array}{c}(X_i-X_j)(N_i-N_j)+(X_i^2+X_j^2)\Gamma+(\sigma_i+\sigma_j)N_iN_j\\ -\dfrac{1}{3}[\sigma_i(N_i+\Gamma X_i)^2+\sigma_j(N_j+\Gamma X_j)^2]\end{array}\right\}\\ +r^2\left\{\begin{array}{c}\dfrac{X_i}{\sigma_i}(N_i+\Gamma X_i)+\dfrac{X_j}{\sigma_j}(N_j+\Gamma X_j)+N_iN_j\\ -\dfrac{1}{2}[(N_i+\Gamma X_i)^2+(N_j+\Gamma X_j)^2]\end{array}\right\}\\ +r^4\left\{\dfrac{(N_i+\Gamma X_i)^2}{6\sigma_i^2}+\dfrac{(N_j+\Gamma X_j)^2}{6\sigma_j^2}\right\}\end{array}\right\}, \tag{A2}$$

when $|\sigma_i-\sigma_j|/2 \leqslant r < (\sigma_j+\sigma_i)/2$. The parameters X_i, N_i, and Γ are calculated numerically from

$$X_i = \frac{Z_j}{1+\Gamma\sigma_i} - \frac{c\sigma_i^2}{1+\Gamma\sigma_i}\frac{\displaystyle\sum_{j=1}^{N}\frac{\rho_j^b\sigma_j Z_j}{1+\Gamma\sigma_j}}{1+c\displaystyle\sum_{j=1}^{N}\frac{\rho_j^b\sigma_j^3}{1+\Gamma\sigma_j}}, \tag{A3}$$

$$X_i = Z_i + N_i\sigma_i, \tag{A4}$$

$$\Gamma^2 = \frac{\beta\pi e^2}{\varepsilon}\sum_{i=1}^{N}\rho_i^b X_i^2, \tag{A5}$$

where

$$c = \frac{\pi}{2\left[1-\dfrac{\pi}{6}\displaystyle\sum_{i=1}^{N}\rho_i^b\sigma_i^3\right]}. \tag{A6}$$

[1] R. J. Ellis and A. P. Minton, Nature (London) **425**, 27 (2003).
[2] A. P. Minton, Biophys. Chem. **57**, 1 (1995).
[3] C. W. Liu, A. Lomakin, and G. M. Thurston *et al.*, J. Phys. Chem. **99**, 454 (1995).
[4] H. Mahadevan and C. K. Hall, AIChE J. **36**, 1517 (1990).
[5] J. Rescic, V. Vlachy, L. B. Bhuiyan *et al.*, J. Chem. Phys. **107**, 3611 (1997).
[6] J. Rescic, V. Vlachy, L. B. Bhuiyan, *et al.*, Mol. Phys. **95**, 233 (1998).
[7] J. Rescic, V. Vlachy, C. W. Outhwaite *et al.*, J. Chem. Phys. **111**, 5514 (1999).
[8] C. W. Outhwaite, L. B. Bhuiyan, and V. Vlachy, Mol. Phys. **83**, 183 (1994).
[9] L. B. Bhuiyan, V. Vlachy, and C. W. Outhwaite, Int. Rev. Phys. Chem. **21**, 1 (2002).
[10] Y. X. Yu, J. Z. Wu, and G. H. Gao, J. Chem. Phys. **120**, 7223 (2004).
[11] A. R. Kinjo and S. Takada, Phys. Rev. E **66**, 031911 (2002).
[12] A. R. Kinjo and S. Takada, Phys. Rev. E **66**, 051902 (2002).
[13] Y. X. Yu and J. Z. Wu, J. Chem. Phys. **119**, 2288 (2003).
[14] Y. X. Yu and J. Z. Wu, J. Chem. Phys. **117**, 10156 (2002).
[15] R. Roth, R. Evans, A. Lang, *et al.*, J. Phys.: Condens. Matter **14**, 12063 (2002).
[16] R. Messina, J. Chem. Phys. **117**, 11062 (2002).
[17] Z. X. Tang, L. M. Y. Teran, H. T. Davis, *et al.*, Mol. Phys. **71**, 369 (1990).
[18] Z. X. Tang, L. E. Scriven, and H. T. Davis, J. Chem. Phys. **97**, 9258 (1992).
[19] L. Mieryteran, Z. X. Tang, H. T. Davis, *et al.*, Mol. Phys. **72**, 817 (1991).
[20] C. N. Patra and A. Yethiraj, J. Phys. Chem. B **103**, 6080 (1999).
[21] Y. Rosenfeld, D. Levesque, and J. J. Weis, J. Chem. Phys. **92**, 6818 (1990).
[22] Y. Rosenfeld, J. Phys.: Condens. Matter **14**, 9141 (2002).
[23] Y. Rosenfeld, Phys. Rev. Lett. **63**, 980 (1989).
[24] T. Boublik, J. Chem. Phys. **53**, 471 (1970).
[25] G. A. Mansoori, N. F. Carnahan, K. E. Starling *et al.*, J. Chem. Phys. **54**, 1523 (1971).
[26] K. Hiroike, Mol. Phys. **33**, 1195 (1977).
[27] D. Frenkel and B. Smit, *Understanding Molecular Simulation: from Algorithms to Applications* (Academic, San Diego, 2002).
[28] B. Hribar, V. Vlachy, and O. Pizio, J. Phys. Chem. B **104**, 4479 (2000).

[29] S. N. Petris, D. Y. C. Chan, and P. Linse, J. Chem. Phys. **118**, 5248 (2003).
[30] Y. X. Yu and J. Z. Wu, J. Chem. Phys. **117**, 2368 (2002).
[31] Y. X. Yu and J. Z. Wu, J. Chem. Phys. **118**, 3835 (2003).
[32] C. Gu, G. H. Gao, and Y. X. Yu, J. Chem. Phys. **119**, 488 (2003).
[33] Y. X. Yu and J. Z. Wu, J. Chem. Phys. **116**, 7094 (2002).
[34] Y. P. Tang and J. Z. Wu, J. Chem. Phys. **119**, 7388 (2003).